Chapter 6

A Pair Sum Approximation for Predicting Defect Cluster Binding Energies in Fluorites

Much of the work presented in this chapter has previously been published in Modelling and Simulation in Materials Science and Engineering [145]

6.1 Introduction

As discussed in the introduction, at concentrations beyond the dilute limit defects can no longer be regarded as isolated, instead cluster formation must be investigated. In ionic materials an important term controlling cluster formation is the coulombic interactions between charged defects. The aim of

this study is to realise a model capable of predicting, in a lattice consisting of in excess of 10^6 sites at doping levels up to 1%, the extent to which this clustering will take place and the energetic consequences of such clustering in terms of the resulting structures.

6.1.1 Crystal Structure

Ceria is one of many structures with the formula RX_2,, where R is a cation (either di- or tetra-valent) and X is an anion. Such compositions are likely to have the fluorite structure when the ratio of their radii, $r(\mathrm{R})/r(\mathrm{X}) \geq 0.73$ [146]. This structure has FCC cation packing and the tetrahedral interstices filled by anions, as illustrated by 6.1. Thus, the system has cubic symmetry and exhibits the space group *Fm3m*, in which the ions occupy the Wyckoff positions [147] shown in table 6.1.

Table 6.1: Wyckoff Positions for the fluorite structure [147].

Species	Wyckoff Position	Co-ordinate
R	(4a)	000
X	(8c)	$\pm\left(\frac{1}{4}\frac{1}{4}\frac{1}{4}\right)$

6.1.2 The CeO_2-Gd_2O_3 System

Due to its widespread industrial applications there is an extensive body of simulation work covering ceria. A thorough review of this by Islam and Balducci is available [148]. Of particular relevance to this materials application

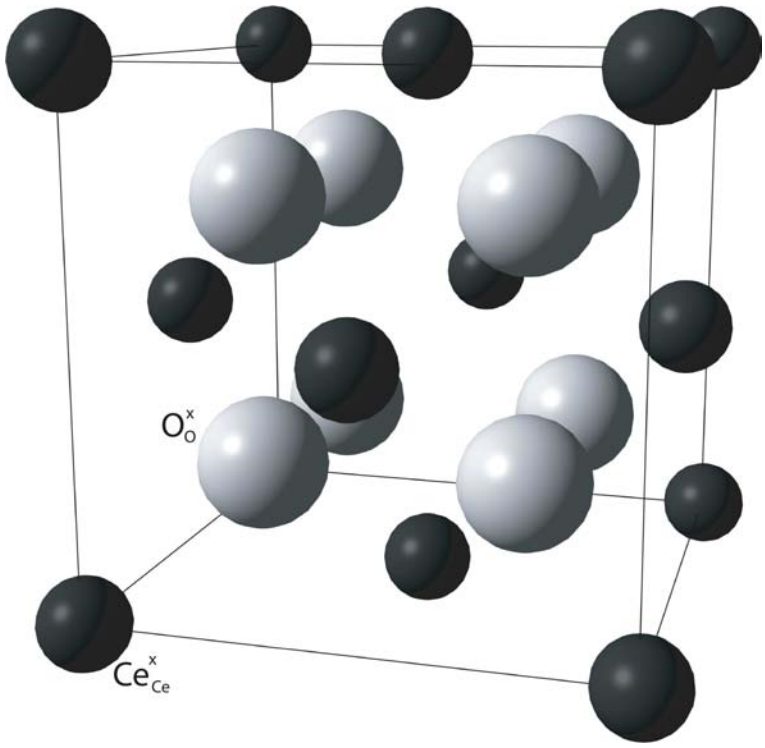

Figure 6.1: Unit cell of Ceria, The Ce^{4+} and O^{2-} ions are represented, respectively, by black and grey spheres.

as a fast ion conductor are calculations of the oxygen vacancy migration energy. Values of 0.74 eV [149], 0.63 eV [150] are in good agreement with experimental evidence [44,151]. The CeO_2-M_2O_3 system in particular has been the subject of a number of theoretical studies such as [67, 152–154] which have emphasised the importance of defect clustering in the determination of conductivity.

Butler *et al.* [153] used atomistic simulation to calculate the energies associated with the clustering of an $V_O^{\cdot\cdot}$ to between 1 and 4 M'_{Ce} defects, for M = (Sc^{3+}, Y^{3+}, Gd^{3+}, Ce^{3+}, La^{3+}). Showing, in accordance with experimental

results, which indicate a peak in the ionic conductivity for a Gd^{3+} dopant, that the cluster binding energy is smallest for M = Gd. Minervini *et al.* [67] repeated these calculations, looking at a larger range of dopants and cluster geometries, the potential set used for these calculations is again employed in this chapter.

Understanding migration in the doped system is more complex, Murray *et al.* [155] used static calculations for CeO_2-Y_2O_3 to generate 30 local environments for an $V_O^{\cdot\cdot}$ surrounded by between 0 and 6 dopant ions. The Monte Carlo method was then used to statistically sample possible migrations, reproducing the experimental maximum in the conductivity. Meyer *et al.* [156] also used Monte Carlo simulations to investigate migration in DO_2-M_2O_3 for a variety of D and M ions. They found that experimental results could be reproduced when a model with reduced transition barriers near dopant ions was used. They explained the results in terms of percolation theory, i.e. at low concentration migration is faster as the migrating ion is surrounded my paths free obstruction (by dopant ions) as concentration increases these paths are filled in.

Previous work on the incorporation of M_2O_3 into ceria [67] and zirconia [157] has shown that the lowest energy solution mechanism involves M^{3+} substituting at cation sites, charge compensated by oxygen vacancies (see figure 6.2). Thus the overall solution reaction is:

$$Gd_2O_3 + 2Ce_{Ce}^{\times} + O_O^{\times} \rightarrow 2Gd_{Ce}^{\prime} + V_O^{\cdot\cdot} + 2CeO_2 \qquad (6.1)$$

In this case the coulomb interations between $V_O^{\cdot\cdot}$ and $Ce_{Ce}^{\times}$ are significant

(this will be demonstrated in section 6.2.1). The consequence of this is that

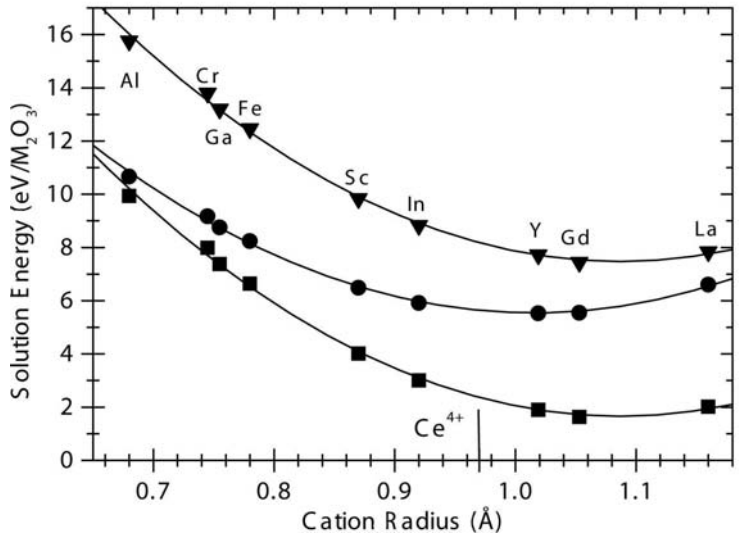

Figure 6.2: Solution energies for incorporation of M_2O_3 in CeO_2, assuming isolated defects, where filled squares denote solution by $V_O^{\cdot\cdot}$ compensation, filled circles - solution by $M_i^{\cdot\cdot\cdot}$ and filled triangles- solution by $Ce_i^{\cdot\cdot\cdot\cdot}$. Reprinted from [67].

a variety of cluster types might form: examples include a pair consisting of a single substitutional cation and an oxygen vacancy $(Gd'_{Ce}{:}V_O^{\cdot\cdot})^{\cdot}$ or a larger neutral cluster $(2Gd'_{Ce}{:}V_O^{\cdot\cdot})^{\times}$ which incorporates two Gd^{3+} species (an example of a neutral trimer is shown in figure 6.3).

In previous work [67] the most stable defect geometry was identified for a variety of single M^{3+} dopants interacting with a single oxygen vacancy. It was found that while dopants of small radii prefer to be in first neighbour sites those with larger radii prefer to form second neighbour geometries. In this regard, for CeO_2, the Gd^{3+} ion is of intermediate size, with only a slight

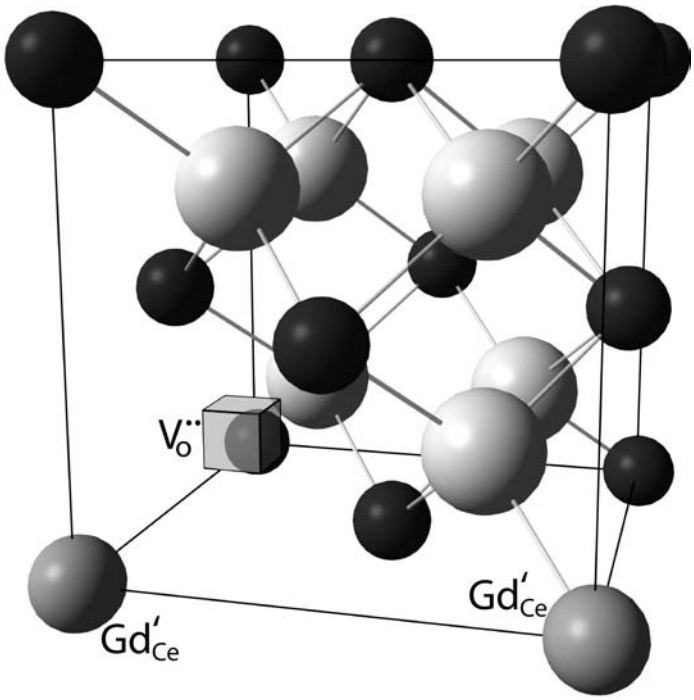

Figure 6.3: Unit cell of fluorite containing an example of a charge neutral $(2Gd'_{Ce}{:}V_O^{\cdot\cdot})^{\times}$ trimer defect. Here one of the Gd'_{Ce} defects is on a first neighbour site relative to the $V_O^{\cdot\cdot}$ while the other is at a second neighbour site.

preference for a second over a first neighbour geometry.

6.1.3 Energy Minimisation

The methodology used to evaluate defect energies in this chapter is that described in section 2.7. The Buckingham potential parameters used are reported in Table 6.2. The values of these parameters were chosen to reproduce the unit cell volumes of various related oxides, for example $La_2Ce_2O_7$ and have previously be used to reproduce the perfect lattice properties of ceria [67].

Table 6.2: Short-range potential parameters [67].

Species	A(eV)	ρ(Å)	C(eV.Å^{-6})
$O^{2-}-O^{2-}$	9547.92	0.2192	32.00
$Ce^{4+}-O^{2-}$	1809.68	0.3547	20.40
$Gd^{3+}-O^{2-}$	1885.75	0.3399	20.34

Ionic polarisability is introduced via the shell model as described in section 2.5; the relevant parameters are reported in Table 6.3.

Table 6.3: Shell model parameters.

Species	Y(eV)	k(eV.Å^{-2})
$O^{2-}-O^{2-}$	-2.04	6.3
$Ce^{4+}-O^{2-}$	-0.20	177.84

Calculations described in this chapter were performed with the CASCADE

code [121].

6.1.4 Cluster Binding Energies

The binding energy, BE, is the difference between formation energies of the sum of the isolated defects (comprising a cluster) and the defect formation energy of the cluster itself. It is used to assess the stability of a cluster; a negative value indicates that the cluster is bound.

6.1.5 Defect Interactions Over Large Distances

Cluster calculations of the Mott-Littleton type become computationally prohibitive when the defects involved are separated by more than 10 Å (due primarily to the large region I size required in order that none of the constituent defects approach the region I/IIa interface). Consequently an alternative scheme has been investigated, in which the total interaction energy of defect clusters, consisting of more than two defects, is constructed by summing the specific pair-wise contributions between the constituents. The total defect binding energy (BE_T) is then:

$$BE_T = \sum_{j>i}^{n} \sum_{i=1}^{n} BE_{ij} \tag{6.2}$$

where n is the total number of defects and BE_{ij} is the defect binding energy of the pair $\{i, j\}$. This method will only be useful if pair-wise interactions between defects in a lattice are dominant, as it ignores any higher order

contributions (i.e. the interaction between lattice defects A and B is not greatly changed by the presence of another lattice defect C).

6.1.6 A Coulombic Approximation for the Pair Interactions

In the defect pair interaction approximation described above defect-defect interactions between pairs of defects are still computed explicitly, using the energy minimisation simulation technique. A more simple, and easily computable model of cluster binding energy would be to use a coulombic approximation such that the binding energy of a constituent pair of defects i and j is:

$$E(r_{ij}) = \frac{1}{4\pi\epsilon_0\epsilon_r}\frac{q_i q_j}{r_{ij}} \tag{6.3}$$

where r_{ij} is the separation of ions i and j (as defined by their unrelaxed lattice positions), q_i and q_j are their excess defect charges and ϵ_r is the relative dielectric constant of the material under consideration. In the next section we shall consider, for the example of Gd_2O_3 doped CeO_2, the limit of application of: (1) the coulomb approximation for the interaction between pairs of defects and, (2) the deconvolution of the larger cluster into its pair components.

6.2 Results and Discussion

6.2.1 The Coulombic Approximation

Three pairs of defects, $(Gd'_{Ce}{:}V^{\cdot\cdot}_{O})^{\cdot}$, $(Gd'_{Ce}{:}Gd'_{Ce})''$ and $(V^{\cdot\cdot}_{O}{:}V^{\cdot\cdot}_{O})^{\times}$ have been considered in detail. These are the only pairs that will occur in this model of Gd_2O_3 doped CeO_2 and as such their binding energies will later form the basis for the pair deconvolution analysis.

Figures 6.4-6.6 show the variation of binding energy with separation for the three dimers. The points on the graphs each correspond to an explicit

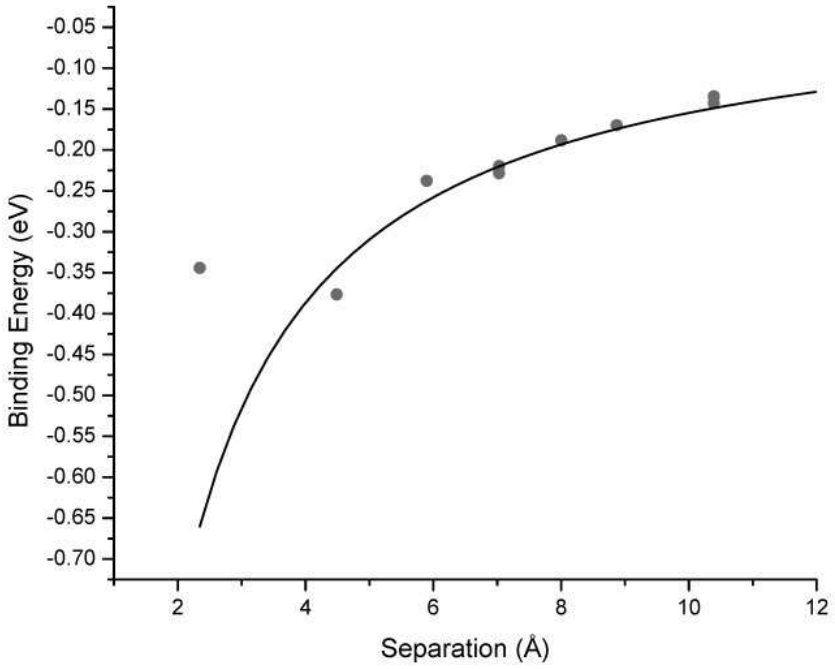

Figure 6.4: Binding energy (eV) as a function of separation (Å) for a$(Gd'_{Ce}{:}V^{\cdot\cdot}_{O})^{\cdot}$ pair. Points indicate actual atomistic calculations, the line corresponds to equation 6.3. The negative value indicates that the pair is bound.

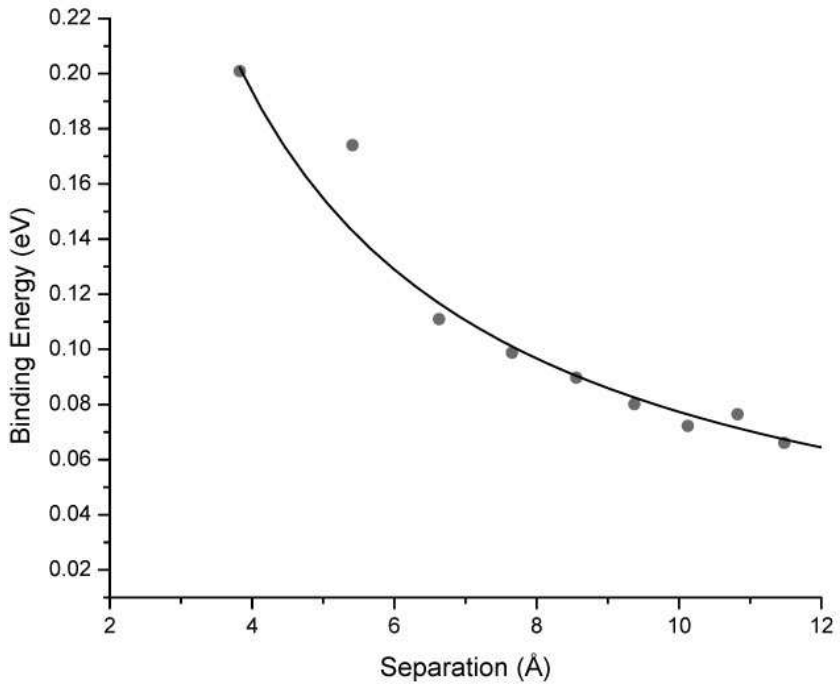

Figure 6.5: Binding energy (eV) as a function of separation (Å) for a(Gd'_{Ce}:Gd'_{Ce})″ pair. Points indicate actual atomistic calculations, the line corresponds to equation 6.3. The positive value indicates that the interaction is repulsive.

Mott-Littleton determined binding energy for a cluster at a defined separation. The separations correspond to first neighbour sites, second neighbour sites and so on. The lines on the graphs correspond to the coulombic approximation (equation 6.3) with the value of ϵ_r calculated using the model parameters (tables 6.2 and 6.3). Thus in each figure 6.4-6.6, the extent to which the points deviate from the line is a measure of accuracy of the coulombic approximation, at that separation, for those particular defects. It is to be expected that the approximation will become increasingly accu-

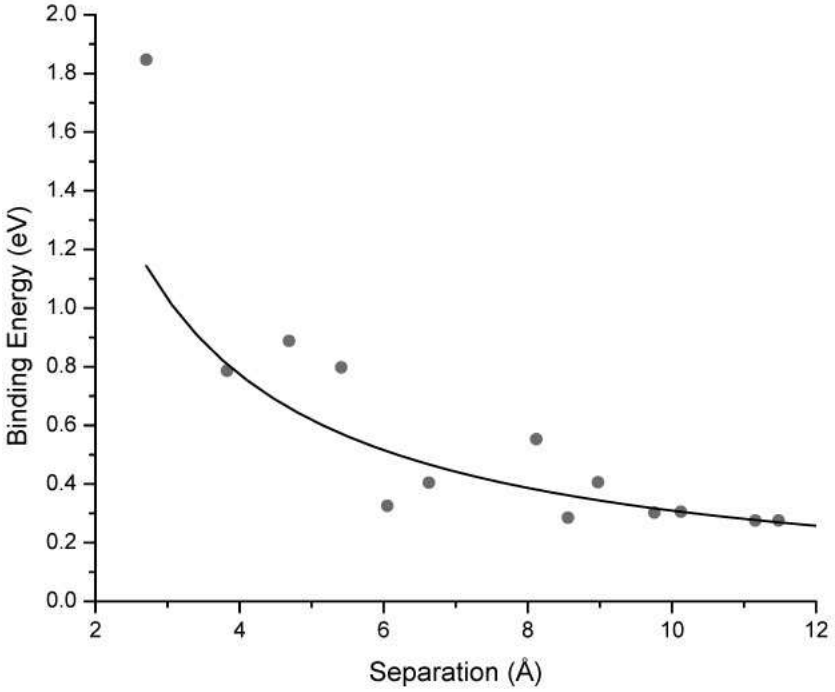

Figure 6.6: Binding energy (eV) as a function of separation (Å) for a $(V_{\ddot{O}}:V_{\ddot{O}})^{\cdots\cdot}$ pair. Points indicate actual atomistic calculations, the line corresponds to equation 6.3. The positive value indicates that the interaction is repulsive.

rate at larger defect separation and this is indeed observed (at larger defect separation lattice relaxation is almost the same as for the isolated defects). In the cases where the defect clusters are $(Gd'_{Ce}{:}V^{\cdot\cdot}_{O})^{\cdot}$ and $(Gd'_{Ce}{:}Gd'_{Ce})''$ the convergence is rapid: Once the species are separated by just four lattice sites (i.e. approximtely 6 Å) the deviation is within 4% of the binding energy for subsequent $(Gd'_{Ce}{:}V^{\cdot\cdot}_{O})^{\cdot}$ separations and within 5% for $(Gd'_{Ce}{:}Gd'_{Ce})''$. In the case of $(V^{\cdot\cdot}_{O}{:}V^{\cdot\cdot}_{O})^{\cdot\cdot\cdot\cdot}$ convergence to the coulombic model requires the defects to be separated by more than 9 Å before the convergence has reached an acceptable level.

6.2.2 The Pair Binding Energy Deconvolution

The simplest neutral cluster is a trimer consisting of two Gd^{3+} substitutional ions and one O^{2-} vacancy, i.e. $(2Gd'_{Ce}{:}V^{\cdot\cdot}_{O})^{\times}$ (an example is shown in figure 6.3). The binding energies for this cluster have been evaluated for 62 different geometries. These include, though are not limited to, all cases in which the largest $Gd'_{Ce}{:}V^{\cdot\cdot}_{O}$ and $Gd'_{Ce}{:}Gd'_{Ce}$ separations are at most fourth neighbour.

The binding energy of the trimer can be considered, according to equation 6.2, as the sum of three pair interactions. We will consider two cases. First, where the pair binding energies are derived from the simple coulombic model (i.e. via equation 6.3). Following this we will consider the extent to which the explicitly calculated pair energies (i.e. those in figures 6.4 - 6.6) reproduce the trimer binding energies for these compact defect clusters.

The Coulombic Approximation for $(2Gd'_{Ce}{:}V^{\cdot\cdot}_{O})^{\times}$ Binding Energies

Figure 6.7 illustrates the performance of the coulombic approximation (equations 6.3).

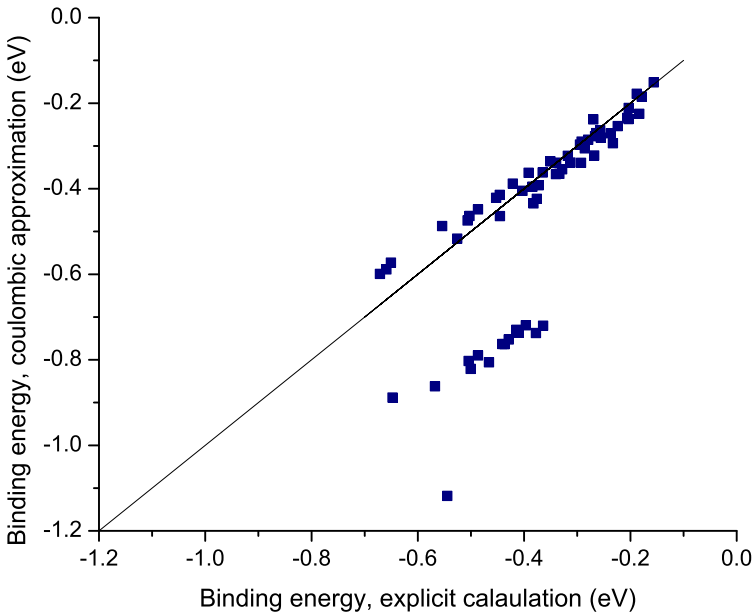

Figure 6.7: Comparison of BE, for different geometries of the $(2Gd'_{Ce}{:}V^{\cdot\cdot}_{O})^{\times}$ cluster. Ideally all points would lie on the solid line x=y, indicating that the BE found via explicitly relaxing the trimer is equal to that found via the coulombic approximation.

Ideally all points would lie on the solid line x=y, indicating that the binding energy found by explicitly relaxing the trimer is equal to that predicted via the coulombic approximation. The plot shows that there exist two distinct groups, those geometries that fall close to this line and those that do not. Those points falling far below the x=y line all correspond to clusters containing at least one a first neighbour $(Gd'_{Ce}{:}V^{\cdot\cdot}_{O})^{\cdot}$ pair. The point furthest

from the line is that in which all the ions are first neighbours with respect to one another (only one $2Gd'_{Ce}{:}V^{\cdot\cdot}_{O})^{\times}$ cluster in CeO_2 can fulfill this criterion). Geometries that do not contain first neighbour Gd'_{Ce} - $V^{\cdot\cdot}_{O}$ pairs fall close to the line. For these cases, the coulombic approximation differs from the explicit calculation on average by -0.0017eV with a standard deviation of 0.0345eV. It is not surprising that the coulombic approximation fails for first neighbour geometries because, as shown in figure 6.4, it is particularly poor at describing the Gd'_{Ce} - $V^{\cdot\cdot}_{O}$ interaction at this distance.

The Use of Pair Energies from Explicit Calculation for $(\mathbf{2Gd'_{Ce}{:}V^{\cdot\cdot}_{O}})^{\times}$ Binding Energies

Figure 6.8 compares the binding energies predicted via explicit calculation to those predicted via equation 6.2, using pair energies calculated explicitly. Ideally all points would lie on the solid line x=y, indicating that the binding energy found by explicitly relaxing the trimer is equal to that found via summing the contributions from the explicit pair interactions. The average discrepancy between the two methods is 0.0004 eV with a standard deviation of 0.0121 eV for all cluster geometries.

The result marked by a triangle represents the case where all the defects are first neighbours (it is worth noting that this is not among the most stable cluster configurations). It might have been anticipated that this would be the most difficult case for the pair summation to reproduce and so it proves; explicitly relaxing the cluster produces a more stable structure than

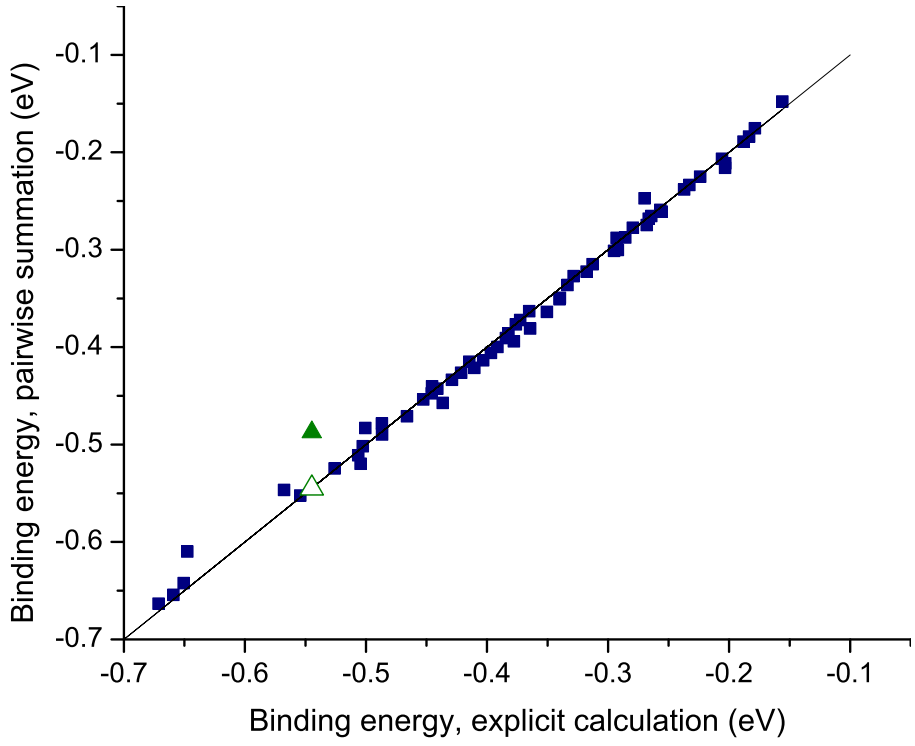

Figure 6.8: Comparison of binding energy, for different geometries of the $(2\mathrm{Gd}'_{\mathrm{Ce}}{:}\mathrm{V}_{\ddot{\mathrm{O}}})^{\times}$ cluster. The green triangle represents the case where all the constituent defects lie at first neighbour sites.

anticipated by the pairwise summation. The less satisfactory prediction of the pairwise sum in this specific case can be understood in terms of the relaxation of the cluster and in how this relaxation contrasts with how each of the constituent pairs relax in isolation. Table 6.4 contrasts the interdefect separations for this trimer with those found for the relevant dimers. It can be seen that the first neighbour Gd'_{Ce}:$V^{\cdot\cdot}_{O}$ separation is unchanged between the dimer and trimer, however the Gd'_{Ce}:Gd'_{Ce} separation is smaller for the dimer than for the trimer. Thus, we find that the presence of an oxygen vacancy results in a greater Gd'_{Ce}:Gd'_{Ce} relaxation which increases slightly the binding energy of this cluster. This additional energy, E_{ijk} amounts to -0.059 eV per first neighbour trimer. This energy can be used to establish a three-body energy correction for clusters that include such configurations. The scale of this correction is shown in figure 6.8.

Table 6.4: Relaxed ionic separations (Å). The dimer values are those for a first neighbour pair. In determining these separations the $V^{\cdot\cdot}_{O}$ is at the lattice site.

	Gd'_{Ce}:Gd'_{Ce} separation	Gd'_{Ce}:$V^{\cdot\cdot}_{O}$ separation
Dimer	3.79	2.48
Trimer	4.04	2.48

A Greater Challenge for the Pair Approximation: Calculating Binding Energies for $(3Gd'_{Ce}{:}V^{\cdot\cdot}_{O})'$ Clusters

A range of $(3Gd'_{Ce}{:}V^{\cdot\cdot}_{O})'$ cluster geometries have been chosen to further test the pair binding energy approximation. Special attention is paid to those which contain a single first neighbour (Gd'_{Ce} - $V^{\cdot\cdot}_{O}$ - Gd'_{Ce}) component (an example of such a cluster may be found in figure 6.9). Furthermore, the cluster that contains *three* first neighbour (Gd'_{Ce} - $V^{\cdot\cdot}_{O}$ - Gd'_{Ce}) components was also included (note: it is geometrically impossible to form a $(3Gd'_{Ce}{:}V^{\cdot\cdot}_{O})'$ cluster with only two first neighbour (Gd'_{Ce} - $V^{\cdot\cdot}_{O}$ - Gd'_{Ce}) components). Figure 6.10 illustrates these results in the same manner as figure 6.8. The relaxed pair summation reproduces the explicit relaxation with an average discrepancy of -0.0155 eV and a standard deviation of 0.0521 eV; this is larger than the corresponding deviation for the $(2Gd'_{Ce}{:}V^{\cdot\cdot}_{O})^{\times}$ trimers.

In figure 6.10 the subset of the $(3Gd'_{Ce}{:}V^{\cdot\cdot}_{O})'$ clusters containing one first neighbour (Gd'_{Ce} - $V^{\cdot\cdot}_{O}$ - Gd'_{Ce}) component, are marked by solid triangles and the cluster with three first neighbour (Gd'_{Ce} - $V^{\cdot\cdot}_{O}$ - Gd'_{Ce}) components is denoted by a star. The binding energies for these are clearly less well reproduced than those for clusters with larger defect separations. Consequently the previously defined three body correction is added to the $(3Gd'_{Ce}{:}V^{\cdot\cdot}_{O})'$ binding energies predicted by the pairwise sum, once for each distinct first neighbour (Gd'_{Ce} - $V^{\cdot\cdot}_{O}$ - Gd'_{Ce}) component; the solid triangles in figure 6.10 are then replaced by the hollow ones. The average discrepancy for the $(3Gd'_{Ce}{:}V^{\cdot\cdot}_{O})'$ cluster is thereby reduced to 0.0049eV with a standard deviation is reduced

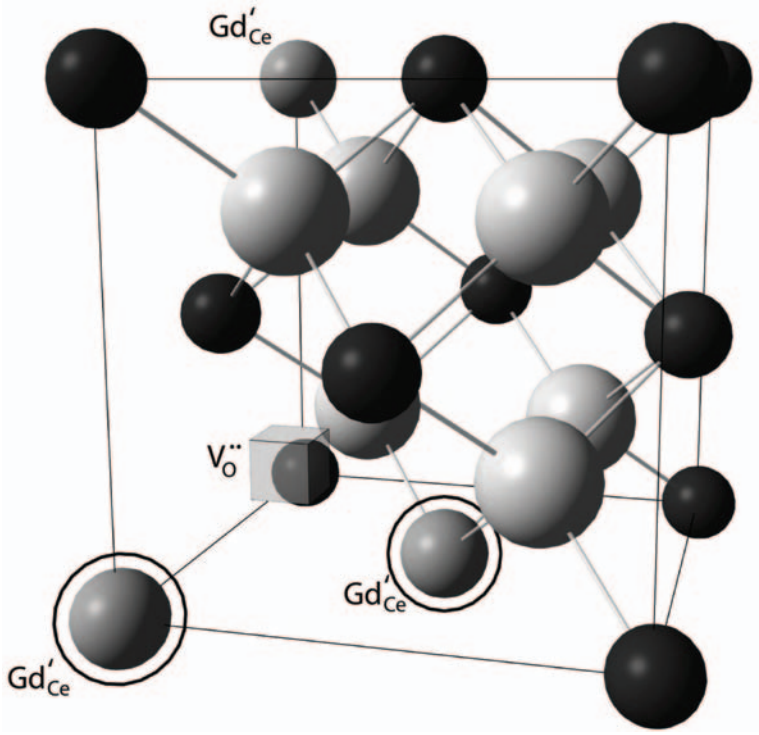

Figure 6.9: Unit cell of CeO_2 with $(3Gd'_{Ce}{:}V_O^{\cdot\cdot})'$ defect, the 2 circled Gd'_{Ce} defects, along with the $V_O^{\cdot\cdot}$ comprise the first neighbour (Gd'_{Ce} - $V_O^{\cdot\cdot}$ - Gd'_{Ce}) component for which the three body correction is required.

to 0.0331eV.

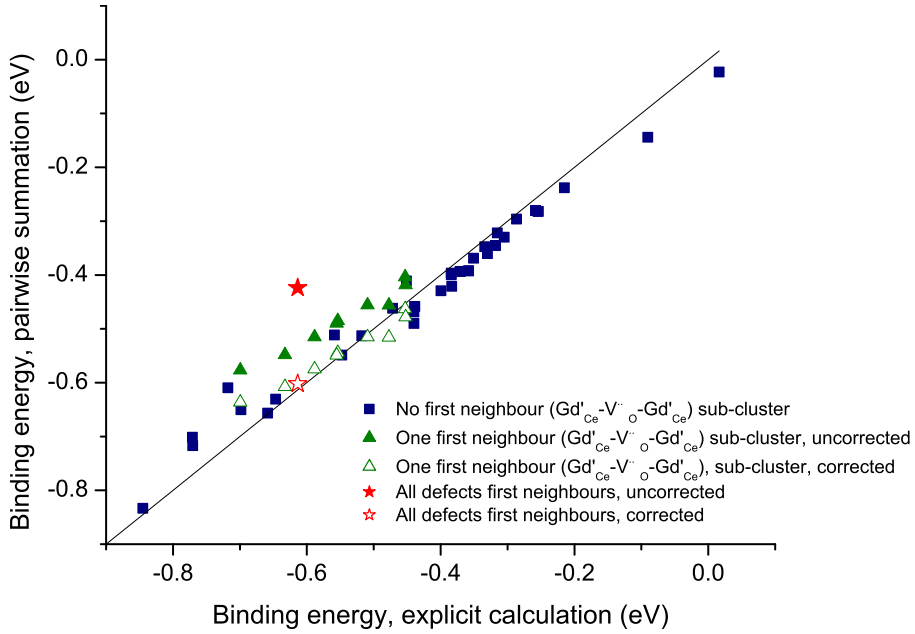

Figure 6.10: Comparison of binding energy, for different geometries of the $(3Gd'_{Ce}{:}V^{\cdot\cdot}_{O})'$ cluster. The triangles represent cases where at least one nearest neighbour (Gd'_{Ce} - $V^{\cdot\cdot}_{O}$ - Gd'_{Ce}) sub-cluster is present. The solid triangles vaules determined via the pairwise sum, the hollow triangles show the predicted binding energy for the same clusters after the three body correction is applied. The cluster with three first neighbour (Gd'_{Ce} - $V^{\cdot\cdot}_{O}$ - Gd'_{Ce}) components is denoted by a star, again solid for the uncorrected case and hollow for the corrected value.

Further conformation of the success of the three body correction can be found by considering an oxygen vacancy surrounded by four first neighbour Gd^{3+} substitutional ions (i.e. a clusters containing five defects). Two configurations were considered. In the first, all Gd'_{Ce} ions are at first neighbour sites

with respect to the $V_O^{\cdot\cdot}$ (it may be that this is the worst possible case for any cluster), in the second all Gd'_{Ce} ions are at second neighbour sites. In table 6.5 the pair only and three body corrected energies are presented for these largest clusters. The first neighbour cluster contains six (Gd'_{Ce} - $V_O^{\cdot\cdot}$ - Gd'_{Ce}) components, consequently the pair sum does not accurately reproduce the explicit cluster calculation.

Table 6.5: Binding energies (eV) for the tetrahedral defect cluster $(4Gd'_{Ce}{:}V_O^{\cdot\cdot})''$.

Geometry	Explicit calculation	Pairwise summation	Corrected summation
First neighbour	-0.555	-0.159	-0.516
Second neighbour	-0.837	-0.812	n/a

Once the three body correction is applied the approximation fares much better, falling within 0.05 eV of the cluster calculation. The second neighbour cluster does not require the three body correction to reproduce the cluster energy. Nevertheless the error in the predicted binding energy for such larger clusters is becoming more significant and suggests that further analysis should be carried out in order to estimate the cluster size (and through configurational entropy arguments, defect concentrations) limit to which this approach is useful.

6.3 Summary

A method has been described whereby the total binding energy of a (geometrically relaxed) defect cluster can be described as a sum of interactions between the cluster's component pairs. In the first instance these pair interactions were calculated assuming the defects interact only through their net coulomb charges, centered at perfect lattice sites. It was found that this crude approximation worked remarkably well if the defects were separated beyond first neighbour sites. Nevertheless, more detailed analysis of defect pair interactions leads to the following criteria for this system: the Coulomb interaction should be used to describe (Gd'_{Ce} - $V^{\cdot\cdot}_{O}$) and (Gd'_{Ce} - Gd'_{Ce}) interactions beyond third neighbour sites and ($V^{\cdot\cdot}_{O}$ - $V^{\cdot\cdot}_{O}$) interactions beyond ninth neighbour sites. For defect pairs within these distances the pair interaction energy should be taken from explicit pair binding energy calculations that include full lattice relaxation.

Analysis of $(3Gd'_{Ce}{:}V^{\cdot\cdot}_{O})'$ clusters showed that better results could be obtained if a three-body correction of each first neighbour (Gd'_{Ce} - $V^{\cdot\cdot}_{O}$ - Gd'_{Ce}) interaction were incorporated into the model. It was shown that the same correction significantly improved the predicted binding energy of a (worst case) $(4Gd'_{Ce}{:}V^{\cdot\cdot}_{O})'$ cluster with six (Gd'_{Ce} - $V^{\cdot\cdot}_{O}$ - Gd'_{Ce}) components but that pair interactions alone were still sufficient to describe a $(4Gd'_{Ce}{:}V^{\cdot\cdot}_{O})'$ that did not contain any such first neighbour components.

For the CeO_2-Gd_2O_3 system the total interaction energy for a n ensemble of

defects can, in this way, be described by carrying out as few as 16 calculations. Previous work on ceria doped with a range of trivalent ions [67] and an equivalent study on doped zirconia [157] suggest the same approach will be successful for all these systems and by inference any fluorite. Of course, if this approach were applied to a crystallographically distinct system the number of explicit defect calculations would not necessarily be the same, it is nevertheless anticipated that the number would remain relatively small.

The approach here provides a significant computational advantage by avoiding the necessity of explicitly calculating energies for the multitude of distinct cluster configurations. Although the effectiveness has been demonstrated for small clusters, further evaluation of the model against larger clusters including those containing multiple vacancies needs to be performed. Nevertheless the present simulations suggest that the approach will be useful for describing fluorite systems with low dopant concentrations (i.e. $<1\%$) where for entropic reasons it is unlikely that larger clusters will form in significant numbers. Conversely, for systems with a different crystallography the possibility of defect clusters with off-lattice site defects (interstitials) would make this approach much more difficult due to the larger number of ill defined configurations.